Bulletin of Geophysics and Oceanography Vol. XX, n. X, pp. XXX-XXX; Xxxxx 20xx
DOI 10.4430/bgo00457

Monitoring crustal movements in Istanbul using GNSS and GIS

M.A. Yücel[1], A. Pirti[2], S. Bayburt[3], Ö. Bektaş[4] and A. Büyüksaraç[5]

[1] *Dept. of Geomatics Engineering, Çanakkale Onsekiz Mart University, Çanakkale, Turkey*
[2] *Dept. of Geomatics Engineering, Yildiz Technical University, Istanbul, Turkey*
[3] *Department of 3D Mapping and GIS, BIMTAS Company, Istanbul, Turkey*
[4] *Dept. of Geophysical Engineering, Sivas Cumhuriyet University, Sivas, Turkey*
[5] *Çan Vocational School, Çanakkale Onsekiz Mart University, Çanakkale, Turkey*

(Received: 23 June 2023; accepted: 4 March 2024; published online: 10 May 2024)

ABSTRACT Istanbul is located south of the Black Sea and north of the Marmara Sea. The seismic stresses and strains in Istanbul and the Marmara Sea are governed by the E-W and NE-SW tectonic characteristics. This research aims to establish the latest crustal motion parameters in Istanbul, utilising Global Navigation Satellite System (GNSS) surveys. A geodetic network was established for this study, comprising 1,159 temporary and nine permanent GNSS stations across Istanbul's Asian and European sectors. Between 2000 and 2020, GNSS measurements were taken, and horizontal and vertical crustal movements and velocity vector maps were produced using GNSS and Geographical Information System (GIS) tools. The GNSS data was processed using GIPSY-OASIS, Topcon Magnet Tools, and Leica Geo-Office software. The data was, then, analysed using ESRI ArcGIS software, which generated thematic maps of Istanbul using ordinary Kriging and trend surface analysis interpolation methods. The analysis results indicate a horizontal variation of the local velocity rate in the SW direction between 14.3 and 17.1 mm per year. Moreover, the data suggests that there is a subsidence variation between -0.7 and -2.0 mm per year. The study results show that the northern block of the North Anatolian Fault Zone moves horizontally towards the SW at an average rate of 16.3 mm per year. The study findings demonstrate a notable horizontal slip rate in the northern regions, whereas vertical subsidence is significantly observable in the eastern regions. The study involved the creation of Voronoi cells for each temporary GNSS station, followed by the calculation of regional shift magnitudes in the area surrounding each station. In regions with notable horizontal and vertical slippage, it would be beneficial to increase the number of observation stations, particularly within the extensive Voronoi cells. The long-term and continuous GNSS measurements greatly improve the study of ongoing crustal movement and tectonic deformation processes in north-western Anatolia.

Key words: Istanbul, crustal movement, earthquake, GNSS, GIS, spatial interpolation.

1. Introduction

Turkey is situated within the Alpine-Himalayan orogenic belt and is among the most seismically active areas in the world (Bozkurt, 2001; Işık *et al*., 2020). The distribution of seismicity is focused on high-strain regions, many of which are major strike-slip faults, such as the North Anatolian Fault Zone (NAFZ), the East Anatolian Transform Fault, and the Western Anatolian Graben zones. The NAFZ is a continuous and narrow fault system that cuts the Anatolian

peninsula in an E-W direction, from Karlıova in the east to the northern Aegean in the west. The NAFZ is a 1,200-kilometre long strike-slip fault zone that connects the east Anatolian convergent zone to the Hellenic subduction zone (Tatar *et al*., 2012; Şengör *et al*., 2014). The distribution of earthquakes that dominate the seismic pattern of the northern part of Turkey, is mostly parallel to the NAFZ (Örgülü, 2011; Poyraz, 2015; Bohnhoff *et al*., 2016). The NAFZ, which is the northern plate boundary of the Anatolian Plate with the N-S extensional regime of the Aegean region, spreads as a complex fault system (dividing two main sections) in the eastern part of the Marmara region, in contrast to the simple structure of the NAFZ (Fig. 1) (Mert *et al*., 2016). Around Bolu, the NAFZ is divided into two parts called the Northern Splay and the Southern Splay, and in the northern section it presents many deformations (Marmara section) (Ergintav *et al*., 2014; Wollin *et al*., 2019). Important conclusions were reached concerning the aeromagnetic anomalies of the Marmara in relation to the geodynamic formation of the Marmara Sea (Ates *et al*., 2008). Accordingly, in the middle part of the Marmara Sea, there is a central ridge horst settlement, probably Palaeozoic/Precambrian in age, similar to the Palaeozoic formations of Istanbul (Ates *et al*., 2003). It can be observed that no major earthquake has occurred along the central ridge. In the north of the Marmara Sea, the presence of very intense magnetic anomalies in the E-W direction is known. These anomalies, caused by wide and shallow magnetised bodies, were modelled and proposed as a vertical dyke model. These magnetised dykes were evaluated as magnetic material filling the fault zones of the northern boundary of the normal faults in the Marmara Sea, reaching a depth of 14-15 km (Ates *et al*., 2008). Conversely, there are counterclockwise block rotations in the north of the Marmara Sea (Ates *et al*., 2009). The last three major earthquakes ($M_W \geq 7$) that occurred on the Marmara section were the Murefte-Ganos

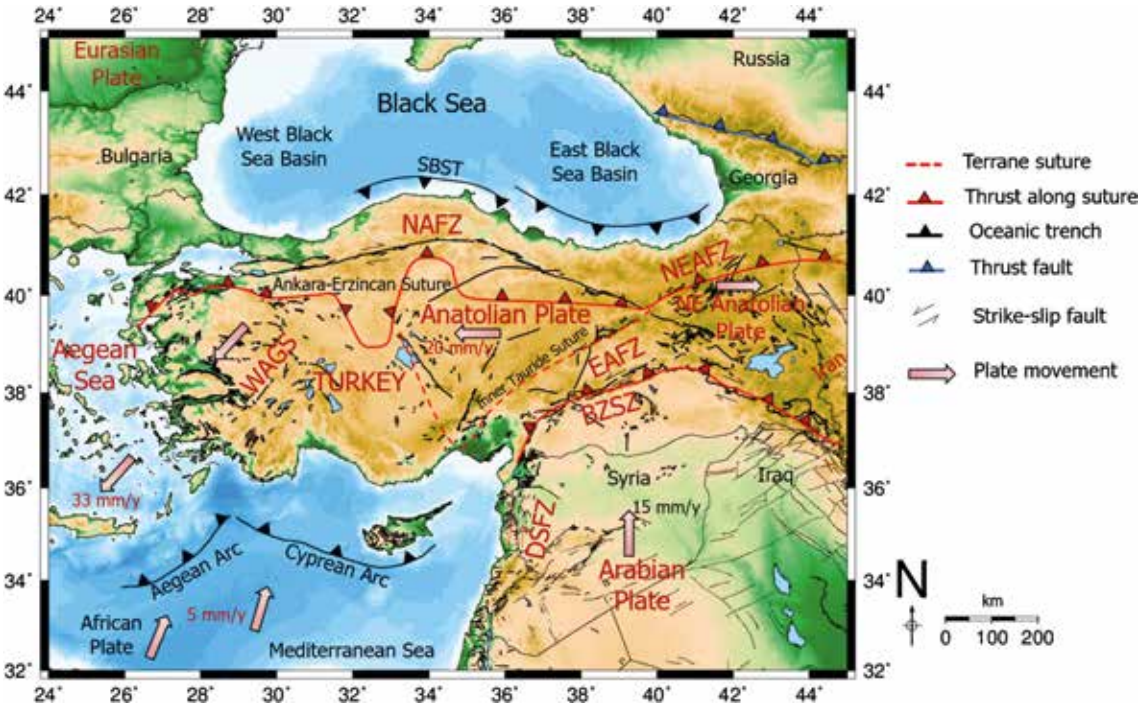

Fig. 1 - Tectonic map of Turkey and the surrounding area: North Anatolian Fault Zone (NAFZ); East Anatolian Fault Zone (EAFZ); NE Anatolian Fault Zone (NEAFZ); Bitlis-Zagros Suture Zone (BZSZ); Dead Sea Fault Zone (DSFZ); Western Anatolian Graben System (WAGS); Southern Black Sea Thrust (SBST) (Alkan *et al*., 2021).

earthquake, in the western part of the region in 1912, and the Izmit and Duzce earthquakes, in the eastern part in 1999 (Ambraseys, 1970; Pinar *et al*., 2001; Barka *et al*., 2002; Janssen *et al*., 2009). The last major historical earthquake in the Marmara section occurred in 1766 (M = 7.4) in the Marmara Sea (Ambraseys, 1970). The estimated recurrence interval of this fault is 200-250 years, and, currently, it is in the final phase of its seismic cycle; thus, it is believed to indicate a seismic gap whose activation as a $M_W \geq 7.0$ earthquake threatens the Marmara region (Parsons, 2004; Bohnhoff *et al*., 2016; Wollin *et al*., 2019).

The Marmara region includes densely populated (over 23 million) and industrial cities in Turkey such as Istanbul, Bursa, and Kocaeli. There is a sizable population in the area that may be affected by an earthquake. On 17 August 1999, the devastating Golcuk earthquake (M_W = 7.4) killed 18,373 people (Kundak, 2023). Some medium-magnitude earthquakes around Istanbul occurred after this date and were localised south of Istanbul. The location of $M_W \geq 5$ earthquakes that occurred in the middle and eastern Marmara Sea from 1999 to 2020 is shown in Fig. 2. In addition, Fig. 3 shows historical and recent earthquakes that occurred in north-western Turkey from 1900 to 2020. Worthy of mention is a trend parallel to the NAFZ that was noticed in the last earthquakes to occur during this period.

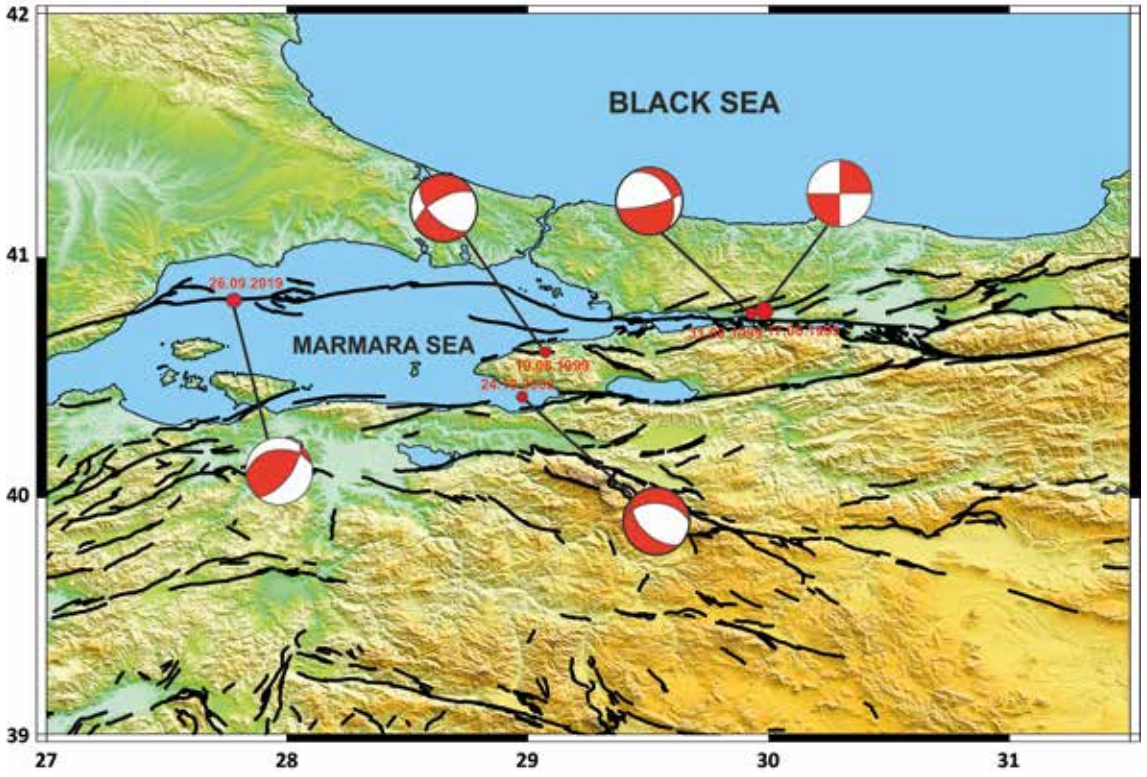

Fig. 2 - Recent earthquakes (M_W > 5) that occurred around the study area between 1999 and 2020 [data collected from Bogazici University - Kandilli Observatory and Earthquake Research Institute (KOERI, 2020)].

The Marmara Sea is an inland sea, 275 km long and 80 km wide, connecting the Black Sea to both the Aegean Sea and the Mediterranean. There is a wide, shallow shelf in the south and sub-basins up to 1,280 m in depth to the north (Sato *et al*., 2004). It is one of the important

regions of the world where historical earthquakes have been reported in the last 1500 years. Over the past 500 years, approximately 28 historical earthquakes (M_S > 6.0) were reported in the Marmara region (Ambraseys and Jackson, 2000; Yaltirak, 2002; Cisternas *et al*., 2004; Erdik *et al*., 2004; Başarır Baştürk *et al*., 2016; Diao *et al*., 2016; Hori *et al*., 2017; Bulut *et al*., 2019). The earthquakes that caused the greatest damage in Istanbul were those of 1509 (Marmara Sea), 1754 (Marmara Sea), and 1766 (Marmara Sea). These three earthquakes are known to have been in the M_S 6.8-7.2 range, with their macroseismic results showing a magnitude smaller than the major earthquakes of 1719 Golcuk (M_S 7.4), 1912 Murefte (M_S 7.3), and 1999 Golcuk (M_S 7.4) in the Marmara region (Ambraseys and Jackson, 1998, 2000; Parke *et al*., 1999). The M_S 6.8 earthquakes reflect 15.3 mm per year of right-side velocity using the global M_S ratio and 12.9 mm per year using the regional velocity (Ambraseys and Jackson, 2000). The velocity calculated from Global Navigation Satellite System (GNSS) measurements is 22 ±3 mm per year in the Marmara region (Straub *et al*., 1997; Ambraseys and Jackson, 2000).

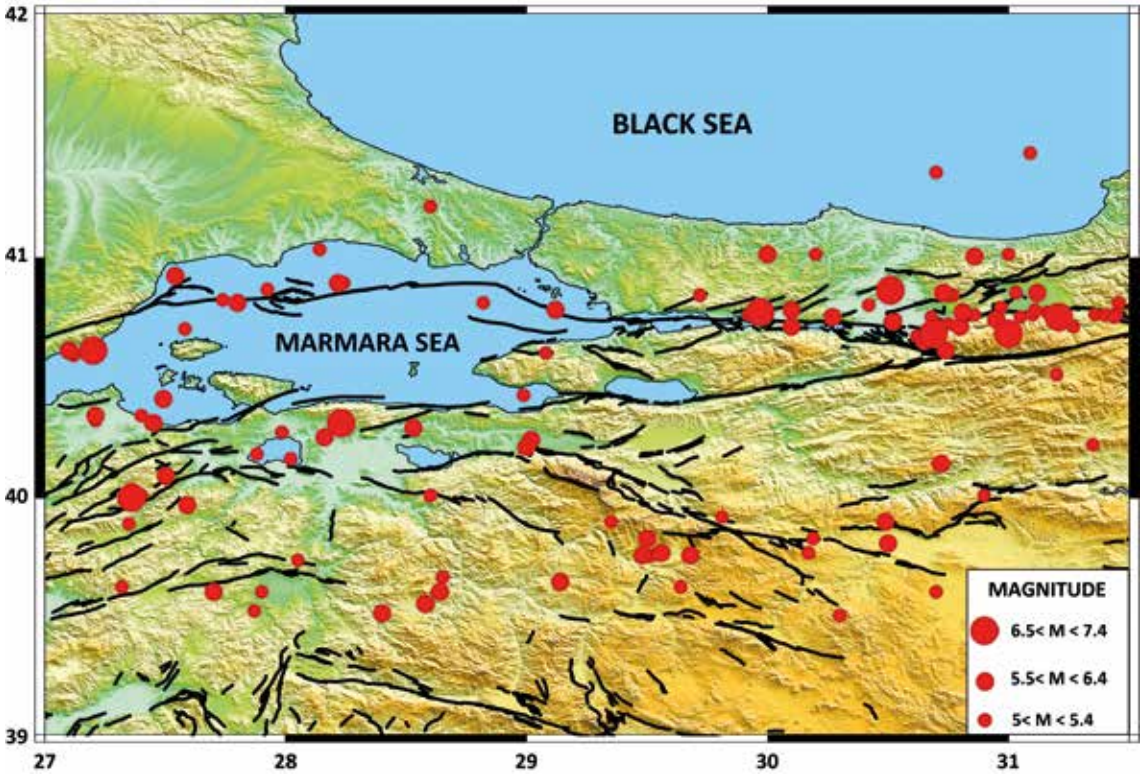

Fig. 3 - Historical and recent earthquakes (*M* > 5) in north-western Turkey between 1900 and 2020 [data collected from Bogazici University - Kandilli Observatory and Earthquake Research Institute (KOERI, 2020)].

McClusky *et al*. (2000) investigated the GNSS measurements for crustal movement at 189 stations on the NAFZ from 1988 to 1997. The Euler vector calculations resulted in a NAFZ slip rate of 24 ±1 mm per year. Motagh *et al*. (2007) instead selected a hybrid of persistent scatterer interferometry (PSI) and GNSS measurements to investigate the crustal movements on the Ganos fault of the NAFZ. They used radar data between 1992 and 2003 and observations from seven GNSS stations. Özyasar and Özlüdemir (2011) calculated the horizontal displacement, ranging

between +18.4 and +89.6 cm, using GNSS measurements from 452 observation stations in Istanbul from 1999 to 2005. Tatar *et al*. (2012) determined the crustal movements of the eastern part of the NAFZ using measurements from 36 GNSS observation stations from 2006 to 2008. They calculated that the slip rate of the NAFZ moves, from east to west, from 16.3 ±2.3 to 24.0 ±2.9 mm per year. Ozener *et al*. (2013) calculated that the average slip rate on the Ismetpasa segment of the NAFZ was 7.6 ±1 mm per year from 2005 to 2011 GNSS station observations.

Istanbul is Turkey's most highly populated city, with an estimated population of more than 15 million people. The city is very crowded and includes many historical places and tourist attractions, as well as large industrial areas. It includes the continents of Europe and Asia, and the Bosporus runs from north to south through the city. The city area is approximately 5.5 km^2, with a population density of 2,900 people per km^2. Therefore, it is important to investigate crustal motions and seismicity in this densely populated city. The aim of this study was to determine the latest crustal motion parameters in Istanbul using GNSS surveys. The study area is located along the Black Sea and Marmara Sea, between latitudes 40°47' N and 41°36' N and longitudes 28°00' E and 29°55' E.

In this paper, the spatial pattern of crustal deformations and the active tectonic plate displacement in the eastern Marmara section were determined using temporary GNSS and continuous GNSS station surveys in Istanbul. For this purpose, densely and almost homogeneously distributed observation stations were used to determine the crustal movements and define the geodetic indications of major earthquakes in the last 20 years. Coordinates were obtained in 2000 and 2020 from 1,168 GNSS stations of the Istanbul network. Data analyses and observations include the widespread GNSS network and long-term data collection and modelling in Istanbul. Thus, the characteristics of horizontal and vertical crustal movements in Istanbul over the last two decades were evaluated using ordinary Kriging and trend surface analysis interpolation methods.

2. Materials and methods

2.1. GNSS surveys and processing by using the ISKI-CORS Network

The velocity vector derived from GNSS measurements offers a precise depiction of the current activity within the Marmara region (McClusky *et al*., 2000; Flerit *et al*., 2004; Özyasar and Özlüdemir, 2011; Erkoç and Doğan, 2023). The methodology adopted in this study involves integrating scientific findings on long-term displacement and fault geometry using the velocity vectors obtained from GNSS locations. This integration enables a precise calculation of the current slip rates on the principal structures. The temporary GNSS station observation data (not online) used was acquired from the Istanbul Metropolitan Municipality. The temporary GNSS stations in Istanbul are distributed in a relatively uniform manner across the city. During both the 2000 and 2020 measurement sessions, a total of 1,168 observation stations were used. These stations consisted of nine permanent Istanbul Water and Sewerage Administration (ISKI) Cross-Origin Resource Sharing (CORS) sites, along with 1,159 temporary stations. The computations took into consideration nine permanent GNSS stations, from the ISKI CORS network, situated in areas of Istanbul (see Fig. 4). The GNSS observations were conducted at the ISKI CORS stations for a duration of 30 minutes, with measurements taken at 1-second intervals. GNSS measurements are usually conducted using 8-hour records; however, due to the high number of stations observed in this particular study, measurements were instead conducted using 30-minute recordings (1-second intervals). The investigation included Topcon HiPer HR and GeoMax receivers. The positive direction of displacement was assumed for displacements in the W-E, S-N, and vertical upward

components. The temporal resolution of the GNSS receivers is 30 s. The ISKI CORS network consists of eight permanent observation stations and one central processing station, which are used for the processing and transmission of GNSS data. The purpose of developing these stations was to construct a precise geodetic network of active stations. These permanent stations are designed to concurrently monitor visible GNSS satellites and facilitate the connection between satellite receivers and permanent GNSS stations. The GNSS receivers transmit tracking data to the central processing station at a computation interval of one second, using either the Internet or the GSM network. The use of the ISKI CORS network is aimed at improving and broadening the capabilities of the GNSS to facilitate the investigation of contemporary crustal displacements. Additionally, it enables undertaking real-time and post-processing investigations on atmospheric and geodynamic phenomena while reducing uncertainty and noise to reveal small-scale movements. The GNSS observations underwent data processing by utilising the GIPSY-OASIS (NASA-JPL, California,

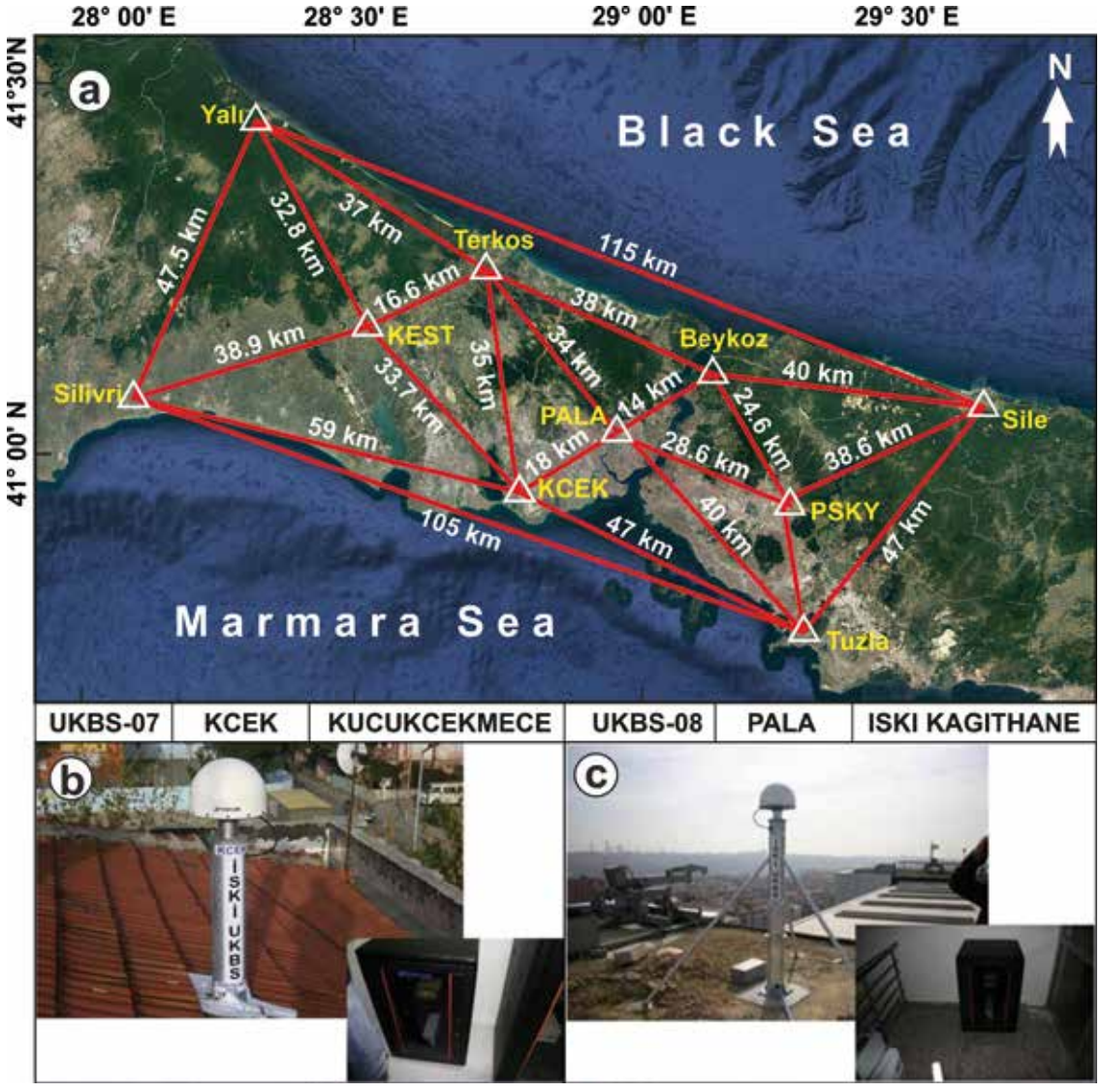

Fig. 4 - a) ISKI CORS GNSS network; b) Kucukcekmece station; c) Kagithane station.

USA) software combination approach. The GIPSY-OASIS program utilises orbit characteristics, Earth rotation parameters, zenith delay to calculate relative position coordinates for observation stations, phase inaccuracy, and the least-squares technique in raw data. The GIPSY-OASIS software was used to establish a connection between the geographical coordinates of the regional GNSS network and the worldwide network. The primary data for GIS (Geographic Information System) analysis consisted of GNSS tracking results spanning the 2000-2020 timeframe.

The processed data shows the mean log components of the coordinate differences between the stations. The displacement velocity patterns in the study area are determined for the subsequent timeframe as a linear tendency of coordinate variations in millimetres per year. The analysis and interpolation of displacement velocity were calculated over the whole area of Istanbul, including 1,168 stations located within the geographical coordinates of 40°45'-41°40' N and 28°-30° E. Additionally, maps depicting the vectors of vertical and horizontal velocity were constructed. In addition, vertical and horizontal velocity vector maps were generated. The coordinates of 1,168 permanent reference stations were measured in Universal Transverse Mercator projection and International Terrestrial Reference Frame 1996 (ITRF96) reference frames in 2000 and 2020. The x-axis, y-axis, and horizontal and vertical changes of the coordinates were calculated using ArcGIS software.

2.2. Spatial interpolation techniques

Spatial interpolation is a geometrical method aiming to calculate the value at a location or area where the value is undefined based on known data (Chen and Guo, 2017). These techniques focus on geographical variables obtained from point sources that provide spatially continuous surfaces over the whole study area. The Kriging technique, pioneered by Krige (Krige, 1951), focuses on the statistical characteristics and weights of a region. The spatial structure of the collected data is the source of the Kriging weights, which are deduced from the estimated spatial structure of the sampled data. The estimated values for locations not observed are found by applying the Kriging weights to the known data values at the locations observed (Krige, 1951; Grzywna *et al*., 2016; Xiao *et al*., 2016; Anand *et al*., 2020; Moraga, 2023). According to Bogusz *et al*. (2014), the Kriging method can handle local changes in the velocity field, adapt well to how the velocity residue values are spread out in space, and accurately detect trends in data. Ordinary Kriging is a geostatistical interpolation method that assumes that the mean of the provided data is unknown and estimated during the interpolation process. This method, which calculates values for linear functions, helps to reduce data variability (Wong *et al*., 2004; Zhu, 2016; Liu *et al*., 2017; Sówka *et al*., 2020). According to Oliver and Webster (1990), the traditional Kriging approach served as the interpolation method for producing velocity field maps.

Trend surface analysis (TSA) uses polynomial functions to construct an interpolation model (Oldham and Sutherland, 1955; Watson, 1971; Sen, 2016). In both local and global contexts, the search is conducted for the surface that is ideally constructed. The global TSA uses all calculated values to determine which polygon is the best (Demir and Tugrul, 2018). In contrast, the local TSA approach only relies on the values seen by neighbouring entities to construct the statistical model. Over time, the trend surface exhibits gradual improvement and effectively captures intricate patterns in the data. In the present context, the process of data interpolation was conducted using ArcGIS spatial analysis tools, specifically the trend technique and the ordinary Kriging method. The goal of the trend interpolation technique is to bring the interpolated polynomial, representing a smooth surface, to be as big as possible. Spatial analysis tools, organising the interplay between the trend method (capturing overarching trends) and the ordinary Kriging method (providing a more localised perspective) come to the forefront. These tools and this

method, working in consistency, allow analysts to visualise raw data, transforming them into insightful and visually appealing maps and models that aid in understanding complex spatial relationships and patterns. In this study, the parameters used for the ordinary Kriging method, using ArcGIS, are given in Table 1.

Table 1 - Parameters for the ordinary Kriging method in displacement coordinates.

Displace-ment	ME	RMSE	S. vario. model	Range (m)	Lag size	Nugget	Sill	Nugget/ Sill	DD
x-axis	-0.000001	0.0005	G	21,794.68	2,724.34	0.000000032	0.000031669	0.001	Strong
y-axis	-0.000013	0.0020	G	19,197.73	2,399.72	0.000001144	0.000133278	0.009	Strong
Horiz.	-0.000010	0.0020	G	18,332.14	2,291.51	0.000001081	0.000119475	0.009	Strong
Vert.	0.000005	0.0006	G	1,5598.58	1,949.82	0.000000007	0.000007161	0.001	Strong

ME: mean error, RMSE: root-mean-square error, G: Gaussian, DD: degree of dependence.

2.3. Voronoi diagrams

Spatial segmentation is a method of splitting a geographic region into a limited number of simultaneously nonoverlapping sub-regions according to specific criteria or constraints that may have various physical or spatial characteristics or relationships. These criteria and constraints can encompass a wide range of physical or spatial attributes and relationships, making spatial segmentation a versatile tool for various applications. One of the notable approaches to achieving spatial segmentation is through the utilisation of Voronoi diagrams. Voronoi diagrams, also referred to as Thiessen polygons, are a fundamental mathematical concept that serves as a foundation for spatial segmentation. In this approach, the primary goal is to determine the closest points within a vast data set and, subsequently, define the regions associated with each of these points using Voronoi cells. The boundaries of the Voronoi cells are determined by considering the distances between each data point and its closest neighbouring points (Moreno-Regidor *et al*., 2012; Pokojski and Pokojska, 2018; Laarhoven, 2021). Voronoi diagrams find applications in a diverse range of fields, including cartography, computational geometry, geography, anthropology, archaeology, astronomy, biology, chemistry, and urban planning (Mota *et al*., 2014; Wang *et al*., 2014; Feng and Murray, 2018). This analysis aids in understanding patterns, clusters, and relationships within the data. Voronoi diagrams were utilised to analyse the impact area of each observation station in this study, which covered a vast area. In surface analysis, Voronoi diagrams were selected as an efficient technique for identifying the domain of a given data set. As a result, it was possible to determine the area that the change impacted on at each observation station.

3. Results

3.1. Displacement of GNSS stations in Istanbul

In this study, a geographical analysis of horizontal and vertical displacements was conducted for an extensive network in Istanbul. Basic components, among which coordinates and a covariance matrix obtained from GNSS processing, were used to calculate the displacements of

the stations. The data obtained from some of the network stations, with the longest monitoring periods, was used to include this station in the network. Then, the network, ITRF96 at 1998.0 epoch, was minimally constrained to prevent datum effects inside the internal geometry of the system by fixing the station coordinates. As a result of the comparison of coordinates obtained from the 2000 and 2020 observation periods, the magnitude of the surface deformation at the observation stations was determined. The displacements of stations were estimated with respect to the ISKI CORS stations. Velocity fields were generated and visualised on maps of the study area using the ordinary Kriging method. Horizontal (x-axis and y-axis) and vertical (ellipsoidal heights) differences were used as input data. The maximum x-axis displacement of all stations was 15.9 cm and the minimum was 10.8 cm, from north to south. The maximum displacement of the y-axis was 38.3 cm and the minimum was 31.6 cm, from east to west. The maximum horizontal displacement was 41.0 cm and the minimum was 34.2 cm, from NE to SW. The maximum vertical displacement was -4.9 cm and the minimum was a -1.7 cm subsidence (Table 2). Figs. 5 to 8 display the x-axis (S-N), y-axis (W-E), and horizontal and vertical displacements obtained for all observation stations.

Table 2 - Calculated displacements and velocity values of the study area.

Direction	Displacement in 20 years (cm)			Velocity (mm/year)		
	Minimum	Maximum	Average	Minimum	Maximum	Average
x-axis	10.8	15.9	14.0	4.5	6.6	5.8
y-axis	31.6	38.3	36.6	13.2	16.0	15.3
Horizontal	34.2	41.0	39.2	14.3	17.1	16.3
Vertical	- 1.7	- 4.9	- 2.8	0.7	2.0	1.2

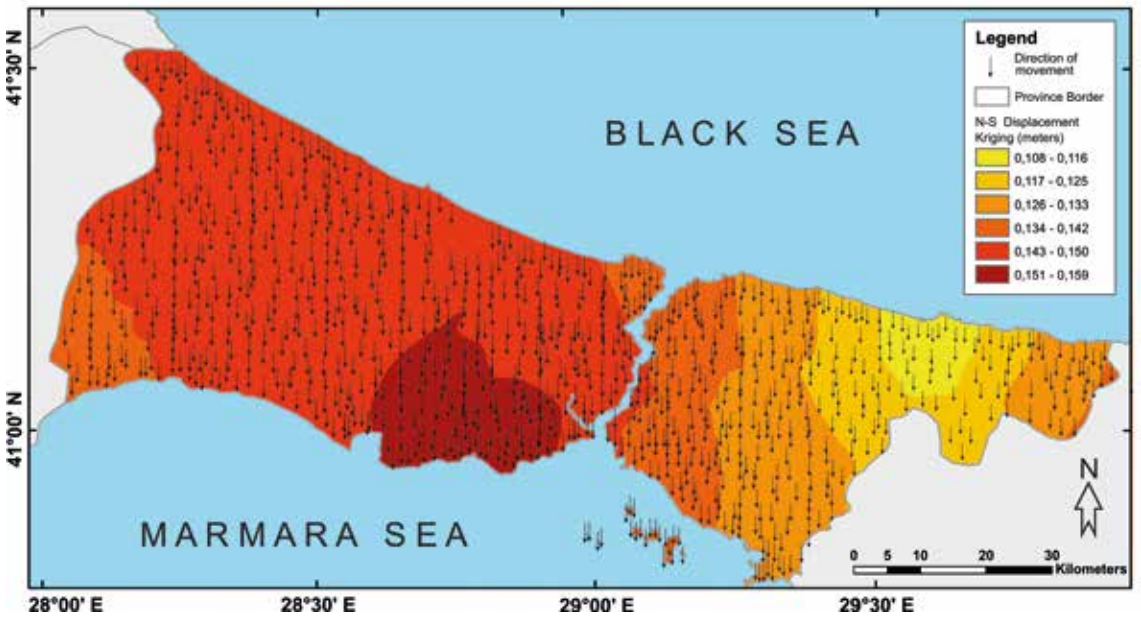

Fig. 5 - X-axis displacements for Istanbul from 2000 to 2020.

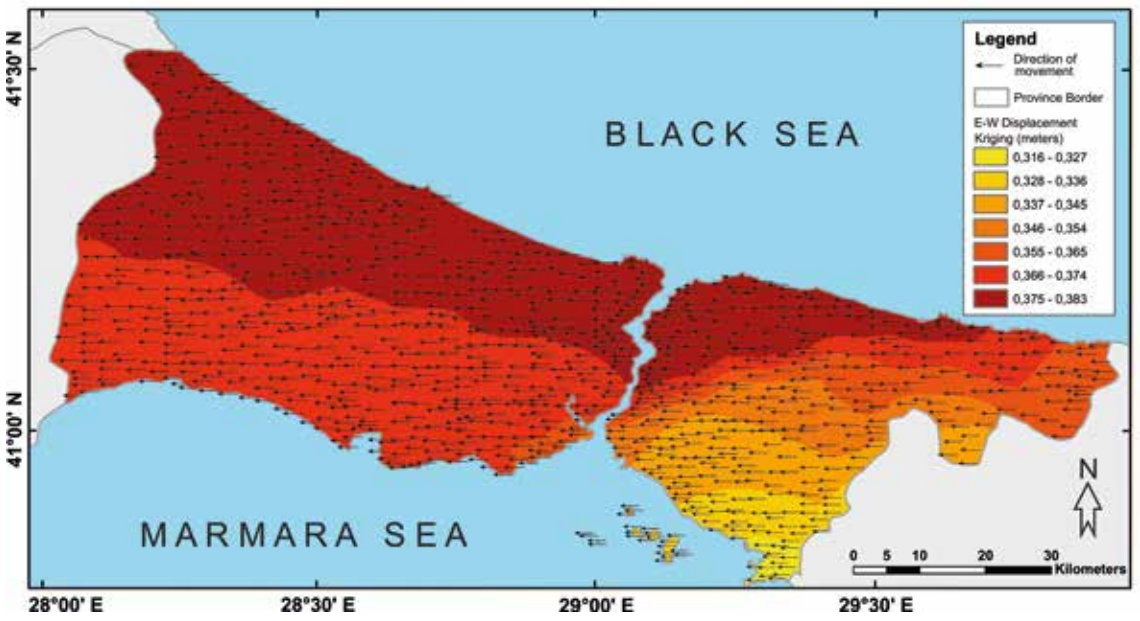

Fig. 6 - Y-axis displacements for Istanbul from 2000 to 2020.

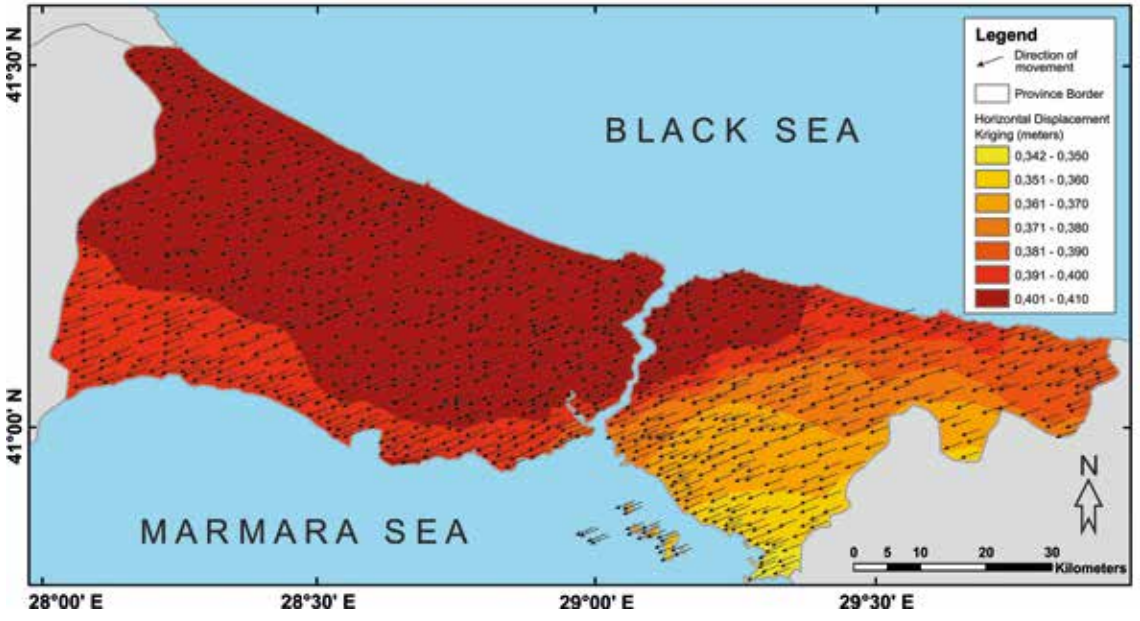

Fig. 7 - Horizontal displacements for Istanbul from 2000 to 2020.

The data set outlined in this study presents data regarding both horizontal and vertical displacements, as well as velocities. The findings gleaned are of great importance to our understanding of tectonic processes and seismic risk assessment. Of note, it is observed that the regional displacement of observation stations, along the x- and y-axes, averages 14.0 cm in the southward direction and 36.6 cm in the westward direction. The data suggest significant lateral

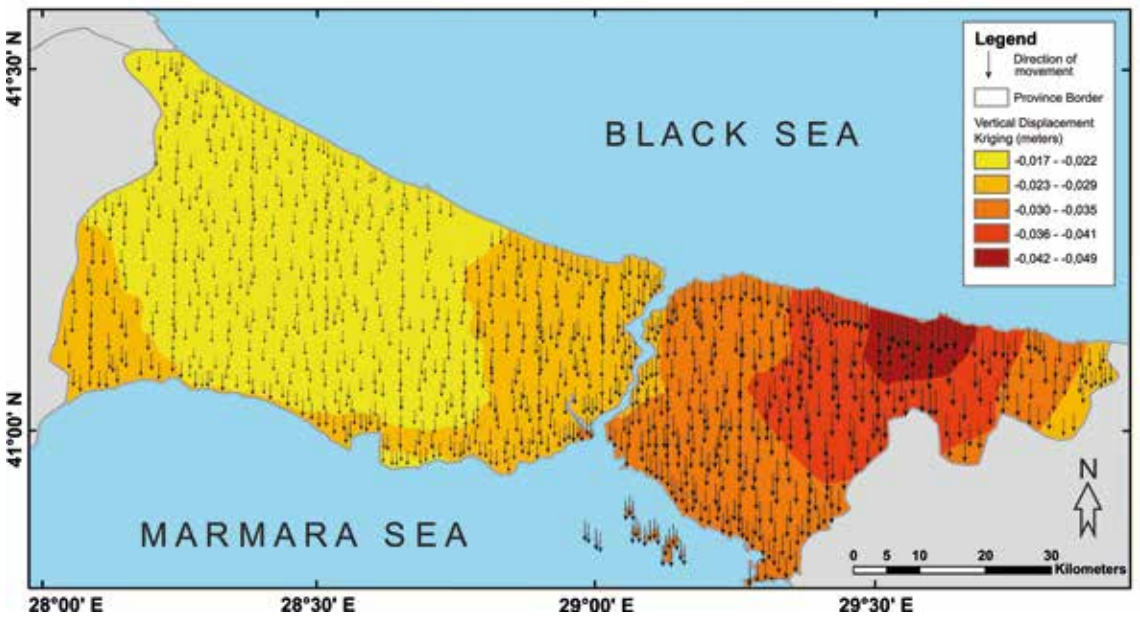

Fig. 8 - Vertical displacements for Istanbul from 2000 to 2020.

shifts experienced by the stations over the past 20 years. The results highlight the complex nature of crustal deformation in the Istanbul area. Additionally, calculating the regional velocities along the x- and y-axes for the stations, which range from 5.8 mm per year in the N-S direction to 15.3 mm per year in the E-W direction, leads to a comprehensive understanding of the constant motion of the Earth's crust in this region. The distinct velocities observed along these two axes could indicate the accumulation of stress on active fault networks. The study found an average horizontal displacement of 39.2 cm, predominantly observed in the NE-SW direction. The mean horizontal velocities of 16.3 mm per year, calculated within the study area, provide significant insight into the crustal dynamics over time. Incorporating the temporal dimension is crucial in assessing seismic hazards.

The regional vertical displacements of the stations exhibit an average subsidence value of -2.8 cm. The subsidence phenomenon poses a considerable challenge for urban planning and infrastructure durability in densely populated cities like Istanbul. As the vertical velocities have been estimated at a rate of -1.2 mm per year, suggesting ongoing subsidence, the implementation of a comprehensive geodetic monitoring system is recommended. It is essential to develop a comprehensive understanding and effectively tackle the potential hazards posed by ground movement. The computations and observations have been meticulously summarised and presented in Table 2, so as to offer a useful reference point for scholars and geoscientists investigating the Istanbul region.

In this study, Voronoi diagrams were used to determine the impact area of the displacements at the observation stations. This resulted in a total of 1,168 Voronoi cells of various sizes, ranging from 0.1 to 19.8 km^2. The average area of the Voronoi cells is 5.6 km^2. Cells with a smaller area indicate that an observation station is close to another station, while cells with a larger area indicate that an observation station is distant from other stations. Therefore, new monitoring stations can be established in areas where large-area Voronoi cells are located. These cells effectively establish distinct geographical areas of impact. The use of this methodology is crucial

for an accurate geodetic analysis and the evaluation of potential hazards. Figs. 9 and 10 exhibit graphical illustrations of horizontal and vertical displacements in the study area using trend surface analysis conducted with the ArcGIS spatial analysis tool. These figures offer captivating depictions of the displacements. The visualisations shown in Figs. 7 and 8 serve as a valuable

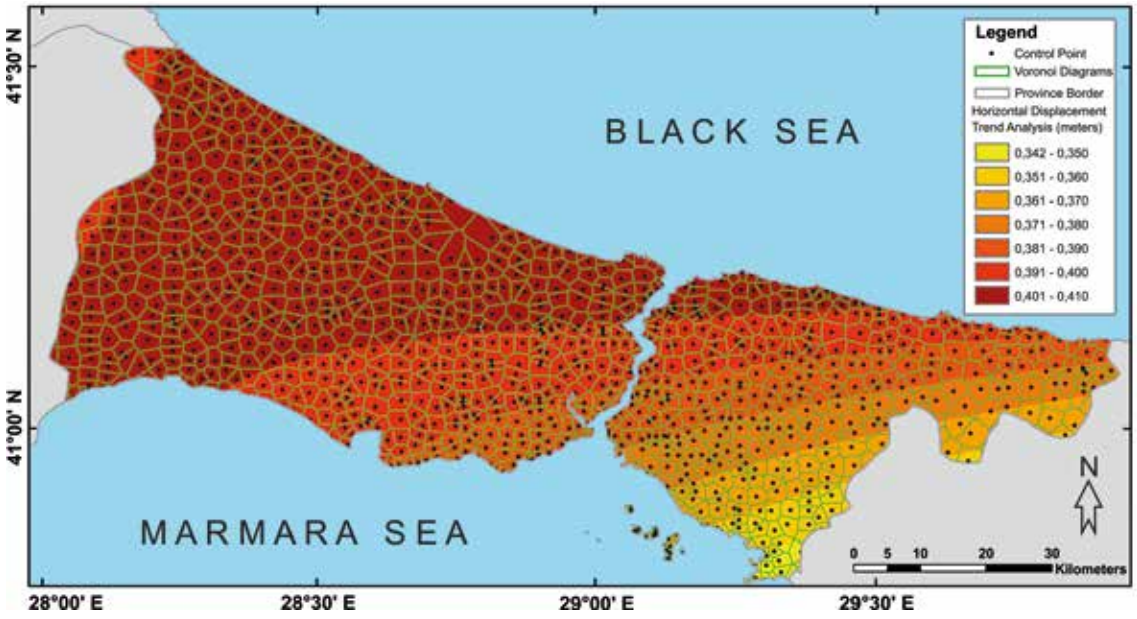

Fig. 9 - Trend analysis results of horizontal displacements and Voronoi diagrams for Istanbul GNSS stations from 2000 to 2020.

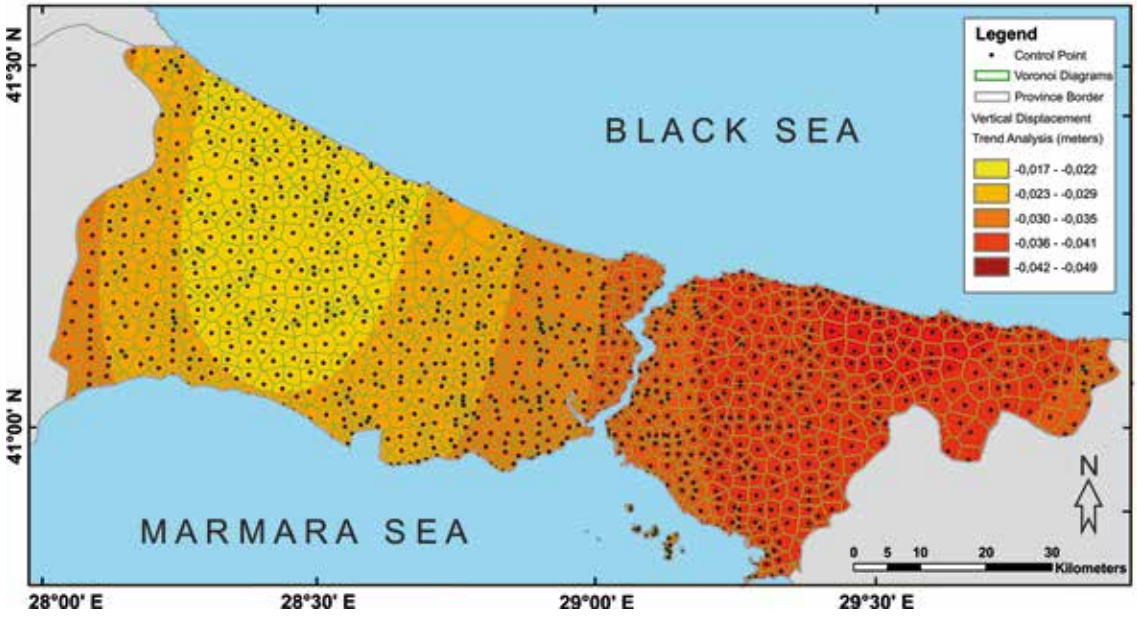

Fig. 10 - Trend analysis results of vertical displacements and Voronoi diagrams for Istanbul GNSS stations from 2000 to 2020.

supplement to the outcomes obtained with the Kriging approach and provide multidimensional viewpoints on the geodetic information, therefore improving its interpretability.

The results of the GIS maps, which were created using spatial analysis tools, show that the study area is moving toward the SW of the region. This movement is parallel to the fault lines in the Marmara Sea and region. In addition, the results show that there is an increase in the amplitude of horizontal displacements at the stations in the western and north-western area and an increase in the modulus of vertical displacements in the eastern and north-eastern coastal regions.

4. Discussion and conclusions

In this study, GNSS monitoring in Istanbul provided accurate descriptions of current crustal movements in the north-eastern part of the Marmara region between the years 2000 and 2020. Velocity vectors and crustal movements were calculated, and the results were visually represented on GIS maps. Also, this study evaluated two different interpolation methods with the results of an ordinary Kriging and TSA. The results of the Kriging and TSA are similar for horizontal and vertical displacements in the study area. Although all the network stations indicate major changes, some stations showed fewer changes during the observation period. During the evaluations, M>5.0 earthquakes, especially the earthquake activity that occurred in the region after the 17 August 1999 earthquake, were taken into account.

According to GNSS measurement results, Istanbul is moving horizontally 16.3 mm every year in a NE-SW direction, parallel to the NAFZ in the Marmara region, and, in fact, a horizontal displacement of 39.2 cm occurred in Istanbul from 2000 to 2020. The movement velocities are non-homogeneously distributed around Istanbul. Relative horizontal displacements in south-eastern Istanbul are smaller than in the other areas (min. 34.2 cm). In addition, the average vertical subsidence movement in Istanbul is 2.8 cm. Conversely, horizontal displacements have increased in the western and north-western areas. Not only does the soil structure affect the displacements, but earthquakes to the east of the Marmara Sea also affect horizontal and vertical displacements. Earthquakes in this area were principally responsible for the increase in the vertical displacement difference in the eastern stations. The NAFZ affecting Istanbul is a strike-slip fault system where, therefore, mostly the y-direction displacement is high (36.6 cm on average) due to the direction of the NAFZ.

On the contrary, the vertical displacement is low, as expected, since there is no mechanism to cause vertical displacement. Another main reason for the vertical displacement is the excessive building construction. A significant vertical displacement occurs with the increase in building mass.

The movement of Istanbul obtained in this study has been confirmed by many researchers (Hergert and Heidbach, 2010; Özyasar and Özlüdemir, 2011; Ergintav *et al*., 2014; Diao *et al*., 2016; Hori *et al*., 2017; Yavasoglu *et al*., 2021) and is compatible with the results of other studies conducted in the region. In their study, Diao *et al*. (2016) reported a horizontal displacement measurement of 18.9 mm per year. According to Ergintav *et al*. (2014), a horizontal displacement from 10 to 15 mm was calculated each year. In the study conducted by Hori *et al*. (2017), the annual displacement was reported to be 2 cm. In addition, Hergert and Heidbach (2010) stated that the slip rate of the main Marmara Fault ranged from 12.8 to 17.8 mm per year and demonstrated high variability along the fault. The annual horizontal displacement was determined to be from 2 to 2.5 cm through the utilisation of GNSS data in the study conducted by Özyaşar and Özlüdemir (2011). Yavasoglu *et al*. (2021) reported displacements ranging from 0.1 to 2.2 mm per year in the section of the NAFZ that involves the provinces of Tekirdag and

Istanbul. The data was obtained from 47 permanent GNSS stations between 2017 and 2020. The agreement between the results of this study and previous studies confirms the accuracy of the measurements, despite the temporal GNSS stations constraint of 30 minutes (1-second intervals) for the GNSS measurements.

Furthermore, this study also included the calculation of vertical displacements, a variable that has been overlooked by other scholars. The utilisation of trend surface analysis for calculating displacements yielded more precise outcomes in both the horizontal and vertical dimensions. Furthermore, the calculation of regional slip amounts was conducted by employing Voronoi diagrams to generate Voronoi cells based on the displacements.

The present research region witnessed the inaugural implementation of this particular methodology. There is a belief that the increase of the frequency (every 3 or 5 years) of GNSS measurements in the field and the accurate determination of long-term displacement quantities and rates can be a viable approach for assessing earthquake risk and stress. Future studies should consider utilising GNSS data to analyse seismic activities using a more extensive network of permanent and temporary GNSS stations. The significance of prospective avenues for future research is duly recognised, with particular emphasis on the integration of GNSS data with seismic activities. The integration of these diverse data sources shows potential for furthering our comprehension of tectonic phenomena. Although the present study does not encompass this aspect, we acknowledge its significance as a promising area for future research. Further investigation in this particular domain is strongly encouraged in order to acquire a more profound understanding of the intricate dynamics within the studied region.

Acknowledgments. We would like to thank the staff at the Istanbul Water and Sewerage Administration (ISKI), Istanbul Metropolitan Municipality-BIMTAS Bosphorus Landscape Build Consultancy Technical Services San. Tic. A.S., Birlik Mapping in Ankara, and Topcon Company for their help in the field. GNSS data used in this research can be requested from the Istanbul Metropolitan Municipality.

REFERENCES

Alkan H., Büyüksaraç A., Bektaş Ö. and Işık E.; 2021: *Coulomb stress change before and after 24.01.2020 Sivrice (Elazığ) earthquake (M_w = 6.8) on the East Anatolian Fault Zone*. Arabian J. Geosci., 14, 2648, 12 pp., doi: 10.1007/s12517-021-09080-1.

Ambraseys N.N.; 1970: *Some characteristic features of the Anatolian fault zone*. Tectonophys., 9, 143-165, doi: 10.1016/0040-1951(70)90014-4.

Ambraseys N.N. and Jackson J.A.; 1998: *Faulting associated with historical and recent earthquakes in the eastern Mediterranean region*. Geophys. J. Int., 133, 390-406, doi: 10.1046/j.1365-246X.1998.00508.x.

Ambraseys N.N. and Jackson J.A.; 2000: *Seismicity of the Sea of Marmara (Turkey) since 1500*. Geophys. J. Int., 141, F1-F6, doi: 10.1046/j.1365-246X.2000.00137.x.

Anand B., Karunanidhi D., Subramani T., Srinivasamoorthy K. and Suresh M.; 2020: *Long-term trend detection and spatiotemporal analysis of groundwater levels using GIS techniques in Lower Bhavani River basin, Tamil Nadu, India*. Environ. Dev. Sustainability, 22, 2779-2800, doi: 10.1007/s10668-019-00318-3.

Ates A., Kayiran T. and Sincer I.; 2003: *Structural interpretation of the Marmara region, NW Turkey, from aeromagnetic, seismic and gravity data*. Tectonophys., 367, 41-99, doi: 10.1016/S0040-1951(03)00044-1.

Ates A., Bilim F., Buyuksarac A. and Bektas Ö.; 2008: *A tectonic interpretation of the Marmara Sea, NW Turkey from geophysical data*. Earth Planet. Space, 60, 169-177, doi: 10.1186/BF03352780.

Ates A., Buyuksarac A., Bilim F., Bektaş Ö., Şendur Ç. and Komanovali G.; 2009: *Spatial correlation of the aeromagnetic anomalies and seismogenic faults in the Marmara region, NW Turkey*. Tectonophys., 478, 135-142, doi: 10.1016/j.tecto.2008.09.025.

Barka A., Akyüz H.S., Altunel E., Sunal G., Çakir Z., Dikbas A., Yerli B., Armijo R., Meyer B., de Chabalier J.B., Rockwell T., Dolan J.R., Hartleb R., Dawson T., Christofferson S., Tucker A., Fumal T., Langridge R., Stenner H., Lettis W., Bachhuber J. and Page W.; 2002: *The surface rupture and slip distribution of the 17 August 1999 İzmit earthquake (M 7.4), North Anatolian Fault*. Bull. Seismol. Soc. Am., 92, 43-60, doi: 10.1785/0120000841.

Başarır Baştürk N., Özel N.M. and Caciagli M.; 2016: *Seismic parameters re-determined from historical seismograms of 1935-Erdek-Marmara Island and 1963-Çlnarclk earthquakes*. Earth Planet. Space, 68, 158, 20 pp., doi: 10.1186/s40623-016-0528-8.

Bogusz J., Kłos A., Grzempowski P. and Kontny B.; 2014: *Modelling the velocity field in a regular Grid in the area of Poland on the basis of the velocities of European permanent stations*. Pure Appl. Geophys., 171, 809-833, doi: 10.1007/s00024-013-0645-2.

Bohnhoff M., Martínez-Garzón P., Bulut F., Stierle E. and Ben-Zion Y.; 2016: *Maximum earthquake magnitudes along different sections of the North Anatolian Fault zone*. Tectonophys., 674, 147-165, doi: 10.1016/j.tecto.2016.02.028.

Bozkurt E.; 2001: *Neotectonics of Turkey – a synthesis*. Geodinamica Acta, 14, 3-30, doi: 10.1080/09853111.2001.11432432.

Bulut F., Aktuğ B., Yaltırak C., Doğru A. and Özener H.; 2019: *Magnitudes of future large earthquakes near Istanbul quantified from 1500 years of historical earthquakes, present-day microseismicity and GPS slip rates*. Tectonophys., 764, 77-87, doi: 10.1016/j.tecto.2019.05.005.

Chen S. and Guo J.; 2017*: Spatial interpolation techniques: their applications in regionalizing climate-change series and associated accuracy evaluation in northeast China*. Geomatics Nat. Hazard Risk, 8, 689-705, doi: 10.1080/19475705.2016.1255669.

Cisternas A., Polat O. and Rivera L.; 2004: *The Marmara Sea region: seismic behaviour in time and the likelihood of another large earthquake near Istanbul (Turkey)*. J. Seismol., 8, 427-437, doi: 10.1023/B:JOSE.0000038451.04626.18.

Demir S. and Tugrul B.; 2018: *Privacy-preserving trend surface analysis on partitioned data*. Knowl. Based Syst., 144, 16-20, doi: 10.1016/j.knosys.2017.12.018.

Diao F., Walter T.R., Solaro G., Wang R., Bonano M., Manzo M., Ergintav S., Zheng Y., Xiong X. and Lanari R.; 2016: *Fault locking near Istanbul: indication of earthquake potential from InSAR and GPS observations*. Geophys. J. Int., 205, 490-498, doi: 10.1093/gji/ggw048.

Erdik M., Demircioglu M., Sesetyan K., Cakti E. and Siyahi B.; 2004: *Earthquake hazard in Marmara Region, Turkey*. Soil Dyn. Earthquake Eng., 24, 605-631, doi: 10.1016/j.soildyn.2004.04.003.

Ergintav S., Reilinger R.E., Çakmak R., Floyd M., Çakır Z., Doğan U., King R.W., McClusky S. and Ozener H.; 2014: *Istanbul's earthquake hot spots: geodetic constraints on strain accumulation along faults in the Marmara seismic gap*. Geophys. Res. Lett., 41, 5783-5788, doi: 10.1002/2014GL060985.

Erkoç M. and Doğan U.; 2023: *Datum definition for geodetic vertical velocity field derived from GNSS observations: a case study in western and southern Turkey*. Bull. Geophys. Oceanogr., 64, 135-148, doi: 10.4430/bgo00412.

Feng X. and Murray A.T.; 2018: *Allocation using a heterogeneous space Voronoi diagram*. J. Geog. Syst., 20, 207-226, doi: 10.1007/s10109-018-0274-5.

Grzywna A., Kamińska A. and Bochniak A.; 2016: *Analysis of spatial variability in the depth of the water table in grassland areas*. Rocznik Ochrona Srodowiska, 18, 291-302.

Hergert T. and Heidbach O.; 2010: *Slip-rate variability and distributed deformation in the Marmara Sea fault system*. Nat. Geosci., 3, 132-135, doi: 10.1038/ngeo739.

Hori T., Pinar A., Necmioglu O., Hori M. and Nishizawa A.; 2017: *Special issue "the next Marmara earthquake: disaster mitigation, recovery, and early warning".* Earth Planet. Space, 69, 65, 4 pp., doi: 10.1186/s40623-017-0648-9.

Işık E., Büyüksaraç A., Ekinci Y.L., Aydın M.C. and Harirchian E.; 2020: *The effect of site-specific design spectrum on earthquake-building parameters: a case study from the Marmara region (NW Turkey)*. Appl. Sci., 10, 7247, 23 pp., doi: 10.3390/app10207247.

Janssen C., Bohnhoff M., Vapnik Y., Görgün E., Bulut F., Schröder B., Pohl D., Aktar M., Okay A. and Dresen G.; 2009: *Tectonic evolution of the Ganos segment of the North Anatolian Fault (NW Turkey)*. J. Struct. Geol., 31, 11-28, doi: 10.1016/j.jsg.2008.09.010.

KOERI; 2020: *Kandilli Observatory and Earthquake Research Institute, Regional Earthquake-Tsunami Monitoring Center*, *Istanbul, Turkey,* <www.koeri.boun.edu.tr/sismo/2/earthquake-catalog/>.

Krige D.G.; 1951: *A statistical approach to some basic mine valuation problems on the Witwatersrand*. J. South Afr. Inst. Min. Metall., 52, 119-139.

Kundak S.; 2023: *Resilience in the shadow of systemic risks*. J. Des. Resilience Archit. Plann., 4, 1-15, doi: 10.47818/DRArch.2023.v4i1079.

Laarhoven T.; 2021: *Approximate Voronoi cells for lattices, revisited*. J. Math. Cryptology, 15, 60-71, doi: 10.1515/jmc-2020-0074.

Liu L., Lin Y., Liu J., Wang L., Wang D., Shui T., Chen X. and Wu Q.; 2017: *Analysis of local-scale urban heat island characteristics using an integrated method of mobile measurement and GIS-based spatial interpolation*. Build. Environ., 117, 191-207, doi: 10.1016/j.buildenv.2017.03.013.

McClusky S., Balassanian S., Barka A., Demir C., Ergintasv S., Georgiev I., Gurkan O., Hamburger M., Hurst K., Kahle H., Kastens K., Kekelidze G., King R., Kotzev V., Lenk O., Mahmoud S., Mishin A., Nadariya M., Ouzounis A., Paradissis D., Peter Y., Prilepin M., Reilinger R., Sanli I., Seeger H., Tealeb A., Toksöz M.N. and Vei G.; 2000: *Global Positioning System constraints on plate kinematics and dynamics in the eastern Mediterranean and Caucasus*. J. Geophys. Res., 105, 5695-5719, doi: 10.1029/1999jb900351.

Mert A., Fahjan Y.M., Hutchings L.J. and Plnar A.; 2016: *Physically based probabilistic seismic hazard analysis using broadband ground motion simulation: a case study for the Prince Islands Fault, Marmara Sea*. Seismol. Earth Planet. Space, 68, 146, 26 pp., doi: 10.1186/s40623-016-0520-3.

Moraga P.; 2023: *Spatial statistics for data science: theory and practice with R.* Chapman and Hall/CRC, New York, NY, USA, 298 pp.

Moreno-Regidor P., García López de Lacalle J. and Manso-Callejo M.Á.; 2012: *Zone design of specific sizes using adaptive additively weighted Voronoi diagrams*. Int. J. Geog. Inf. Sci., 26, 1811-1829, doi: 10.1080/13658816.2012.655742.

Mota D.R., Takano M. and Taco P.W.G.; 2014: *A method using GIS integrated Voronoi diagrams for commuter rail station identification: a case study from Brasilia (Brazil)*. Procedia Soc. Behav. Sci., 162, 477-486, doi: 10.1016/j.sbspro.2014.12.229.

Motagh M., Hoffmann J., Kampes B., Baes M. and Zschau J.; 2007: *Strain accumulation across the Gazikoy-Saros segment of the North Anatolian Fault inferred from Persistent Scatterer Interferometry and GPS measurements*. Earth Planet. Sci. Lett., 255, 432-444, doi: 10.1016/j.epsl.2007.01.003.

Oldham C.H.G. and Sutherland D.B.; 1955: *Orthogonal polynomials: their use in estimating the regional effect*. Geophys., 20, 295-306, doi:10.1190/1.1438143.

Oliver M.A. and Webster R.; 1990: *Kriging: a method of interpolation for geographical information systems*. Int. J. Geog. Inf. Syst., 4, 313-332, doi: 10.1080/02693799008941549.

Örgülü G.; 2011: *Seismicity and source parameters for small-scale earthquakes along the splays of the North Anatolian Fault (NAF) in the Marmara Sea*. Geophys. J. Int., 184, 385-404, doi: 10.1111/j.1365-246X.2010.04844.x.

Ozener H., Dogru A. and Turgut B.; 2013: *Quantifying aseismic creep on the Ismetpasa segment of the North Anatolian Fault zone (Turkey) by 6 years of GPS observations*. J. Geodyn., 67, 72-77, doi: 10.1016/j.jog.2012.08.002.

Özyaşar M. and Özlüdemir M.T.; 2011: *The contribution of engineering surveys by means of GPS to the determination of crustal movements in Istanbul*. Nat. Hazards Earth Syst. Sci., 11, 1705-1713, doi: 10.5194/nhess-11-1705-2011.

Parke J.R., Minshull T.A., Anderson G., White R.S., McKenzie D., Kuşçu I., Bull J.M., Görür N. and Şengör C.; 1999: *Active faults in the Sea of Marmara, western Turkey, imaged by seismic reflection profiles*. Terra Nova, 11, 223-227, doi: 10.1046/j.1365-3121.1999.00248.x.

Parsons T.; 2004: *Recalculated probability of M ≥ 7 earthquakes beneath the Sea of Marmara, Turkey*. J. Geophys. Res. Solid Earth, 109, B05304, 21 pp., doi: 10.1029/2003JB002667.

Pinar A., Honkura Y. and Kuge K.; 2001: *Seismic activity triggered by the 1999 Izmit earthquake and its implications for the assessment of future seismic risk*. Geophys. J. Int., 146, F1-F7, doi: 10.1046/j.0956-540X.2001.01476.x.

Pokojski W. and Pokojska P.; 2018: *Voronoi diagrams - inventor, method, applications*. Pol. Cartogr. Rev., 50, 141-150, doi: 10.2478/pcr-2018-0009.

Poyraz F.; 2015: *Determining the strain upon the eastern section of the North Anatolian Fault zone (NAFZ)*. Arabian J. Geosci., 8, 1787-1799, doi: 10.1007/s12517-014-1301-6.

Sato T., Kasahara J., Taymaz T., Ito M., Kamimura A., Hayakawa T. and Tan O.; 2004: *A study of microearthquake seismicity and focal mechanisms within the Sea of Marmara (NW Turkey) using ocean bottom seismometers (OBSs)*. Tectonophys., 391, 303-314, doi: 10.1016/j.tecto.2004.07.018.

Şen Z.; 2016: *Spatial modeling principles in earth sciences, 2nd ed*. Springer International Publishing, New York, NY, USA, 406 pp., doi: 10.1007/978-3-319-41758-5.

Şengör A.M.C., Grall C., Imren C., Le Pichon X., Görür N., Henry P., Karabulut H. and Siyako M; 2014: *The geometry of the North Anatolian transform Fault in the Sea of Marmara and its temporal evolution: implications for the development of intracontinental transform faults*. Can. J. Earth Sci., 51, 222-242, doi: 10.1139/cjes-2013-0160.

Sówka I., Pawnuk M., Grzelka A. and Pielichowska A.; 2020: *The use of ordinary kriging and inverse distance weighted interpolation to assess the odour impact of a poultry farming*. Sci. Rev. Eng. Environ. Sci., 29, 17-26, doi: 10.22630/PNIKS.2020.29.1.2.

Straub C., Kahle H.G. and Schindler C.; 1997: *GPS and geologic estimates of the tectonic activity in the Marmara Sea region, NW Anatolia*. J. Geophys. Res. B: Solid Earth, 102, 27587-27601, doi: 10.1029/97jb02563.

Tatar O., Poyraz F., Gürsoy H., Çakir Z., Ergintav S., Akpınar Z., Koçbulut F., Fikret Sezen T.F., Türk T., Hastaoglu K.O., Polat A., Mesci L., Gürsoy Ö., Ayazli E., Cakmak R., Belgen A. and Yavaşoğlu H.H.; 2012: *Crustal deformation and kinematics of the eastern part of the North Anatolian Fault zone (Turkey) from GPS measurements*. Tectonophys., 518, 55-62, doi: 10.1016/j.tecto.2011.11.010.

Wang J., Kwan M.P. and Ma L.B.; 2014: *Delimiting service area using adaptive crystal-growth Voronoi diagrams based on weighted planes: a case study in Haizhu District of Guangzhou in China*. Appl. Geog., 50, 108-119, doi: 10.1016/j.apgeog.2014.03.001.

Watson G.S.; 1971: *Trend-surface analysis*. J. Int. Assoc. Math. Geol., 3, 215-226, doi: 10.1007/BF02045792.

Wollin C., Bohnhoff M., Vavrycuk V. and Martínez-Garzón P.; 2019: *Stress inversion of regional seismicity in the Sea of Marmara region, Turkey*. Pure Appl. Geophys., 176, 1269-1291, doi: 10.1007/s00024-018-1971-1.

Wong D.W., Yuan L. and Perlin S.A.; 2004: *Comparison of spatial interpolation methods for the estimation of air quality data*. J. Exposure Anal. Environ. Epidemiol., 14, 404-415. doi: 10.1038/sj.jea.7500338.

Xiao Y., Gu X., Yin S., Shao J., Cui Y., Zhang Q. and Niu Y.; 2016: *Geostatistical interpolation model selection based on ArcGIS and spatio-temporal variability analysis of groundwater level in piedmont plains, northwest China*. Springerplus, 5, 425, 15 pp., doi: 10.1186/s40064-016-2073-0.

Yaltirak C.; 2002: *Tectonic evolution of the Marmara Sea and its surroundings*. Mar. Geol., 190, 493-529, doi: 10.1016/S0025-3227(02)00360-2.

Yavasoglu H.H., Tiryakioglu I., Karabulut M.F., Eyubagil E.E., Ozkan A., Masson F., Klein E., Gulal V.E., Alkan R.M., Alkan M.N., Isiler M. and Arslan A.E.; 2021: *New geodetic constraints to reveal seismic potential of central Marmara region, Turkey*. Bull. Geoph. Ocean., 62, 513-526, doi: 10.4430/bgo00351.

Zhu X.; 2016: *GIS for environmental applications*. *A practical approach* 1st ed. Routledge, London, UK, 490 pp., doi: 10.4324/9780203383124.

Corresponding author: Mehmet ali Yücel
Dept. of Geomatics Engineering, Canakkale Onsekiz Mart University
Prof. Dr. Sevin Buluç Street, Canakkale 17100, Turkey
Phone: +90 286 218 0018; e-mail: aliyucel@comu.edu.tr